Article

Molecular Cell

Distinct Roles for Condensin's Two ATPase Sites in Chromosome Condensation

Graphical Abstract

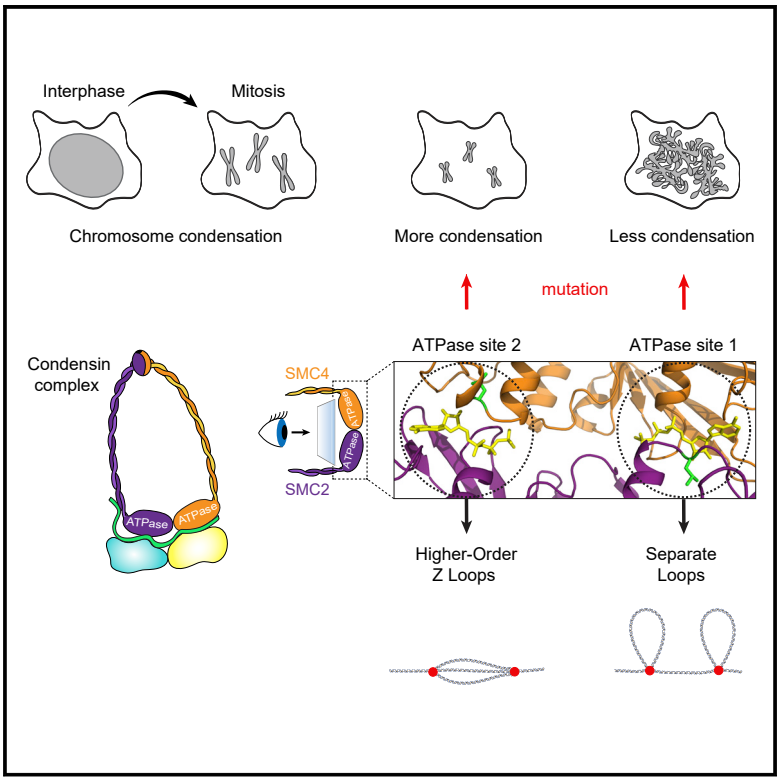

Authors

Ahmed M.O. Elbatsh, Eugene Kim, Jorine M. Eeftens, ..., Christian H. Haering, Cees Dekker, Benjamin D. Rowland

Correspondence

c.dekker@tudelft.nl (C.D.), b.rowland@nki.nl (B.D.R.)

In Brief

Chromosome condensation is essential for accurate cell division. Elbatsh et al. find that condensin's two ATPase sites control condensation through an asymmetric division of tasks. The balanced activity of these sites allows condensin to correctly structure chromosomes. This likely reflects a universal mechanism through which SMC complexes shape genomes in all domains of life.

Highlights

- Condensin's two ATPase sites have distinct roles in structuring chromosomes
- One ATPase site drives loop formation and the second promotes higher-order Z loops
- Hyperactive condensin I shortens mitotic chromosomes in the absence of condensin II
- Condensin II is key to decatenation and forms a straight chromosomal axis

Elbatsh et al., 2019, Molecular Cell *76*, 724–737
December 5, 2019
https://doi.org/10.1016/j.molcel.2019.09.020

CellPress

CellPress

Molecular Cell
Article

Distinct Roles for Condensin's Two ATPase Sites in Chromosome Condensation

Ahmed M.O. Elbatsh,[1,6] Eugene Kim,[2,5] Jorine M. Eeftens,[2,5,7] Jonne A. Raaijmakers,[3,5] Robin H. van der Weide,[1,5] Alberto García-Nieto,[1,5] Sol Bravo,[4] Mahipal Ganji,[2,8,9] Jelmi uit de Bos,[3,10] Hans Teunissen,[1] René H. Medema,[3] Elzo de Wit,[1] Christian H. Haering,[4] Cees Dekker,[2,*] and Benjamin D. Rowland[1,11,*]

[1]Division of Gene Regulation, Netherlands Cancer Institute, Plesmanlaan 121, 1066 CX Amsterdam, the Netherlands
[2]Department of Bionanoscience, Kavli Institute of Nanoscience Delft, Delft University of Technology, Delft, the Netherlands
[3]Division of Cell Biology, Netherlands Cancer Institute, Plesmanlaan 121, 1066 CX Amsterdam, the Netherlands
[4]Cell Biology and Biophysics Unit, European Molecular Biology Laboratory, 69117 Heidelberg, Germany
[5]These authors contributed equally
[6]Present address: Novartis Institutes for Biomedical Research, Klybeckstrasse 141, 4002 Basel, Switzerland
[7]Present address: Department of Chemical and Biological Engineering, Princeton University, Princeton, NJ 08544, USA
[8]Present address: Max Planck Institute of Biochemistry, Martinsried, Germany
[9]Present address: Ludwig Maximilian University, Munich, Germany
[10]Present address: Institute of Biochemistry, Department of Biology, ETH Zürich, 8093 Zürich, Switzerland
[11]Lead Contact
*Correspondence: c.dekker@tudelft.nl (C.D.), b.rowland@nki.nl (B.D.R.)
https://doi.org/10.1016/j.molcel.2019.09.020

SUMMARY

Condensin is a conserved SMC complex that uses its ATPase machinery to structure genomes, but how it does so is largely unknown. We show that condensin's ATPase has a dual role in chromosome condensation. Mutation of one ATPase site impairs condensation, while mutating the second site results in hyperactive condensin that compacts DNA faster than wild-type, both *in vivo* and *in vitro*. Whereas one site drives loop formation, the second site is involved in the formation of more stable higher-order Z loop structures. Using hyperactive condensin I, we reveal that condensin II is not intrinsically needed for the shortening of mitotic chromosomes. Condensin II rather is required for a straight chromosomal axis and enables faithful chromosome segregation by counteracting the formation of ultrafine DNA bridges. SMC complexes with distinct roles for each ATPase site likely reflect a universal principle that enables these molecular machines to intricately control chromosome architecture.

INTRODUCTION

During cell division, the genome undergoes substantial spatial reorganization to allow for its faithful segregation into the newly formed daughter cells. Mitotic chromosome condensation requires the highly conserved condensin complex (Hirano and Mitchison, 1994; Saitoh et al., 1994; Strunnikov et al., 1995). Condensin is an SMC (structural maintenance of chromosomes) protein complex with a ring-shaped structure that at its heart has a heterodimer of SMC2 and SMC4 proteins. Together, these proteins form a composite ABC (ATP-binding cassette)-like ATPase (Hirano, 2016; Uhlmann, 2016). This heterodimer assembles into holocomplexes with three non-SMC subunits. One of these is a member of the kleisin protein family, which together with the SMCs, forms a tri-partite ring. The other two subunits are HEAT-repeat proteins (Haering and Gruber, 2016; Nasmyth and Haering, 2005). Condensin can topologically entrap DNA inside its ring and harbors a second DNA binding interface at one of its HEAT-repeat subunits (Cuylen et al., 2011; Kschonsak et al., 2017).

Metazoans express two distinct complexes, named condensin I and condensin II (Hirota et al., 2004; Ono et al., 2003). The two complexes share the same SMC dimer, but each binds unique kleisin and HEAT-repeat subunits (Figure 1A). The complexes also differ in their cellular localization, abundance, and residence time on chromatin. Condensin II is always nuclear, whereas condensin I is cytoplasmic during most of the cell cycle and only gains access to chromosomes upon nuclear envelope breakdown (NEBD) (Hirano, 2012). During mitosis, condensin II binds to chromosomes with a longer residence time than condensin I, but the former complex is less abundant on mitotic chromosomes than the latter (Gerlich et al., 2006; Walther et al., 2018). In addition to their key role in chromosome condensation, both condensin complexes also regulate sister chromatid resolution (Ono et al., 2013; Piskadlo et al., 2017).

Recent *in vitro* work shows that condensin can create and enlarge DNA loops through a mechanism known as loop extrusion (Ganji et al., 2018). Condensin exerts this key activity in an ATP-dependent manner. The related cohesin complex and bacterial SMC complexes are also thought to act through this mechanism, which somehow involves the ATPase activity of these complexes (Haarhuis et al., 2017; Vian et al., 2018; Wang et al., 2017; 2018). Loop extrusion therefore likely reflects the universal mechanism by which SMC complexes structure genomes in all species (Hassler et al., 2018; van Ruiten and Rowland, 2018).

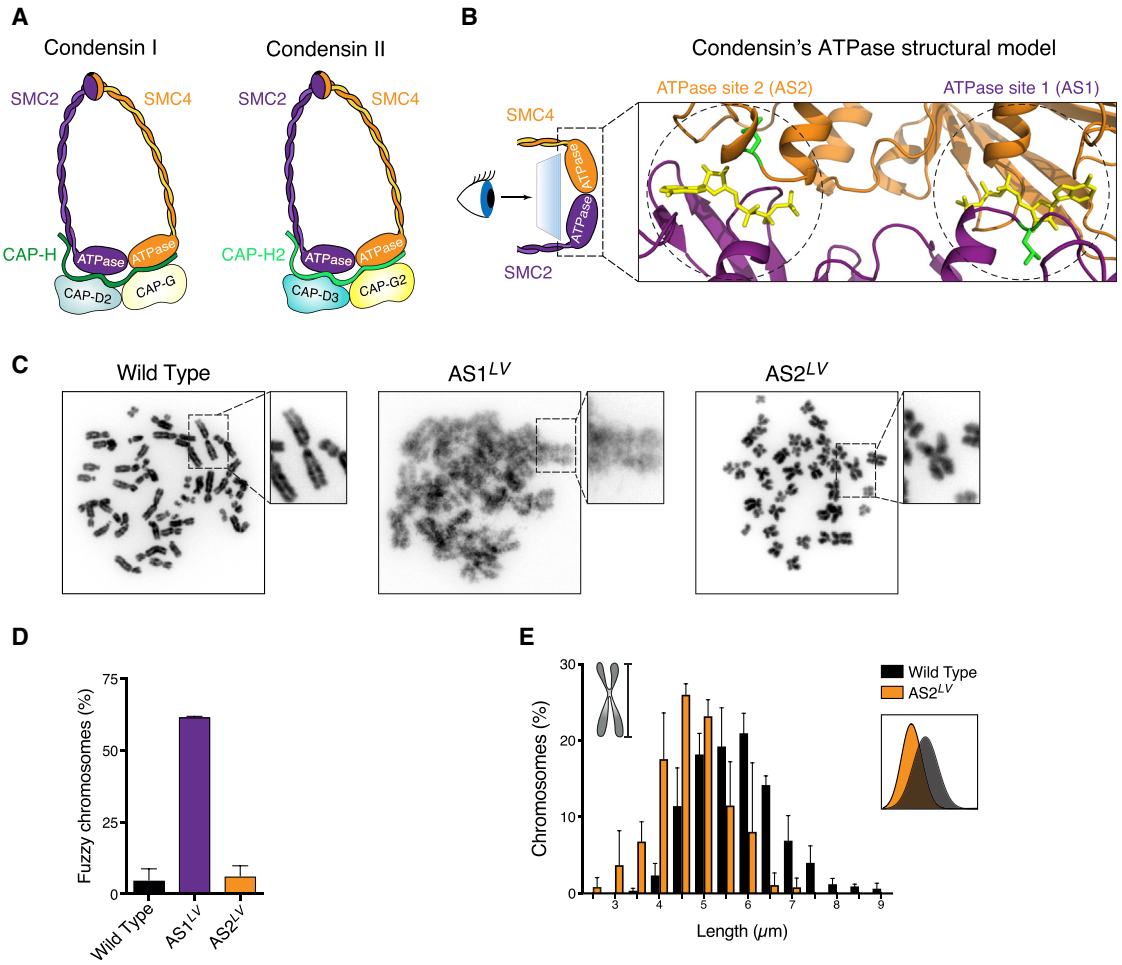

Figure 1. Asymmetric Roles for Condensin's ATPase Sites in Chromosome Condensation

(A) Schematic depiction of metazoan condensin complexes.

(B) Structural model of the SMC2-SMC4 heterodimer. The ATPase head domains of the two proteins engage by sandwiching two ATP molecules (shown in yellow). This yields two composite ATPase sites, which we call ATPase site 1 and 2 (AS1 and AS2, respectively). The model is based on crystal structures of cohesin's Smc1 (PDB: 1W1W) and Smc3 (PDB: 4UX3) subunits. SMC2 is shown in purple and SMC4 in orange. The SMC2 L1085 and SMC4 L1191 residues are highlighted in green.

(C) Representative examples of chromosome spreads of wild-type, AS1^{LV}, and AS2^{LV} mutant cells.

(D) Percentage of mitotic spreads with fuzzy chromosomes of cells shown in (C). The plot shows mean ± SD of three independent experiments of at least 100 spreads per experiment.

(E) Chromosome length measurements of wild-type and AS2^{LV} mutant cells. Chromosomes I, II, and III were measured as in the schematic example. The inset depicts a histogram of the length distribution. The plot shows the mean ± SD of three independent experiments of at least 180 chromosomes per experiment.

How SMC complexes use their ATPase machinery to form DNA loops and structure chromosomes is an important unanswered question. Like all SMC complexes, condensin harbors two ATPase sites (Hirano, 2016). Each of the two sites sandwiches an ATP molecule between the signature motif of one SMC subunit and the Walker A and Walker B motifs of the other (Hopfner, 2016). Here, we reveal a dual role for condensin's conserved ATPase machinery, in which specifically one ATPase site drives, while the other site rather dampens mitotic chromosome condensation. We find that this asymmetric division of tasks is conserved from yeast to humans. We suggest that this mechanism reflects a universal principle for SMC complexes.

RESULTS

Asymmetric Roles for Condensin's ATPase Sites in Chromosome Condensation

To investigate the role of condensin's ATPase in chromosome condensation, we made use of our recently identified ATPase mutants in the cohesin complex that affect its ATPase cycle, but do support viability (Elbatsh et al., 2016). Because the ATPase machineries of cohesin and condensin are very similar, these residues are also conserved among condensin complexes (Figures S1A and S1B). We thus mutated the endogenous allele of each individual ATPase site of condensin (hereafter referred to as AS1 and AS2) in human HAP1 cells using CRISPR/Cas9

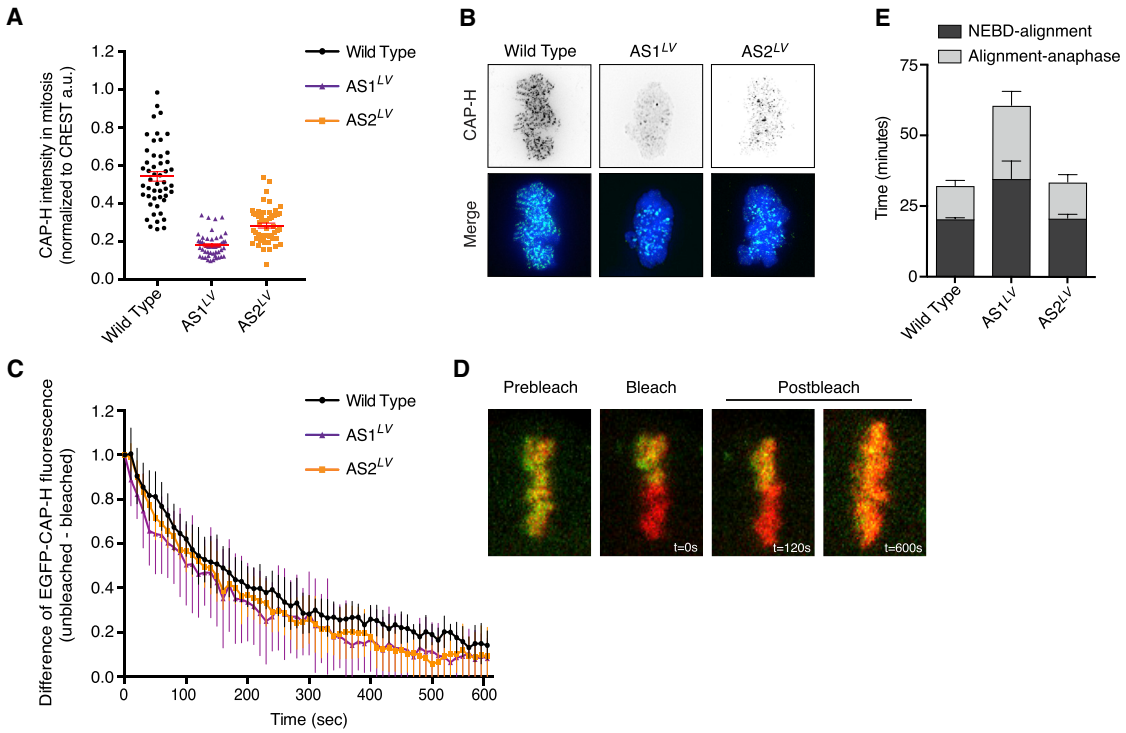

Figure 2. Both ATPase Sites Control Condensin Levels on Chromatin

(A) Quantitative immunofluorescence of chromatin-bound condensin I in wild-type, AS1^{LV} and AS2^{LV} mutant cells. Cells were pre-extracted to remove all unbound condensin. Intensity of CAP-H was measured and normalized over CREST signal. Each dot depicts the signal of one cell. Red line indicates the mean ± SEM of at least 50 cells per condition. The graph is representative of one experiment out of at least 3 independent experiments. See Figure S2 for condensin II levels.

(B) Representative images of mitotic cells stained with CAP-H (green), CREST (cyan), and DAPI (blue) are shown for the cell lines in (A).

(C) Fluorescence recovery after photobleaching (FRAP) experiments on wild-type, AS1^{LV}, and AS2^{LV} mutant cells. Cells were transfected with EGFP-CAP-H 48 h before the experiment. The entire fluorescent signal was bleached except for half of the metaphase plate. Recovery in the bleached and unbleached halves of the plate was followed by time-lapse imaging. DNA was visualized using a DNA probe (SiR-DNA). Curves represent difference in fluorescence signal between bleached and unbleached regions after normalization over DNA signal. n = ≥7 cells from at least two independent experiments. Errors bars represent the SEM

(D) Representative images before (prebleach), at (bleach), or after bleaching (postbleach) for the cells in (C) are shown with the indicated time in seconds.

(E) Live-cell imaging of wild-type, AS1^{LV}, and AS2^{LV} mutant cells. Graph depicts the time spent from nuclear envelope breakdown (NEBD) to alignment and from alignment to anaphase. Cells were labeled with a DNA probe (SiR-DNA) 2 h prior to imaging. The graph shows mean ± SD of three independent experiments with at least 30 cells each.

genome-editing technology (Figures S1C and S1D). These mutations substitute a universally conserved leucine residue of the signature motif of either of condensin's ATPase sites by a valine residue (Figure 1B). We used guide RNAs that led to cleavage of either the *SMC2* or *SMC4* gene and provided donor oligos that, upon homology-directed repair, introduced the desired mutations and at the same time rendered the genes non-cleavable by the Cas9 nuclease. We hereby successfully obtained viable HAP1 cells with mutant endogenous alleles of *SMC2* (AS1^{LV}) and of *SMC4* (AS2^{LV}).

First, we prepared chromosome spreads from wild-type and mutant cells and scored for chromosome condensation. Surprisingly, each mutation led to a very different phenotype. The AS1^{LV} mutation resulted in major condensation defects. The chromosomes of these mutant cells were fuzzy and the individual chromosomes were hard to discern (Figures 1C and 1D). By marked contrast, the AS2^{LV} mutation did not lead to condensation defects. Chromosomes from these mutant cells compacted well and were not fuzzy (Figures 1C and 1D). Upon further examination, we found that AS2^{LV} mutant cells in fact harbored chromosomes that are shorter than those found in wild-type cells (Figure 1E). Importantly, independent mutant clones displayed the same phenotypes (Figures S1E–S1G). The finding that the AS1^{LV} mutation leads to hypo-condensation, whereas the AS2^{LV} mutation results in hyper-condensation, suggests an asymmetric division of tasks between the two ATPase sites in the condensation process.

Both ATPase Sites Control Condensin Levels on Chromatin

We then set out to understand how the AS1^{LV} and AS2^{LV} mutations in condensin lead to these distinct condensation phenotypes. First, we measured the levels of the chromatin-bound fraction of condensin I and II complexes in wild-type and mutant cells (Figures 2A, 2B, S2A and S2B). Interestingly, both mutations reduced condensin levels on chromatin. In each case, the

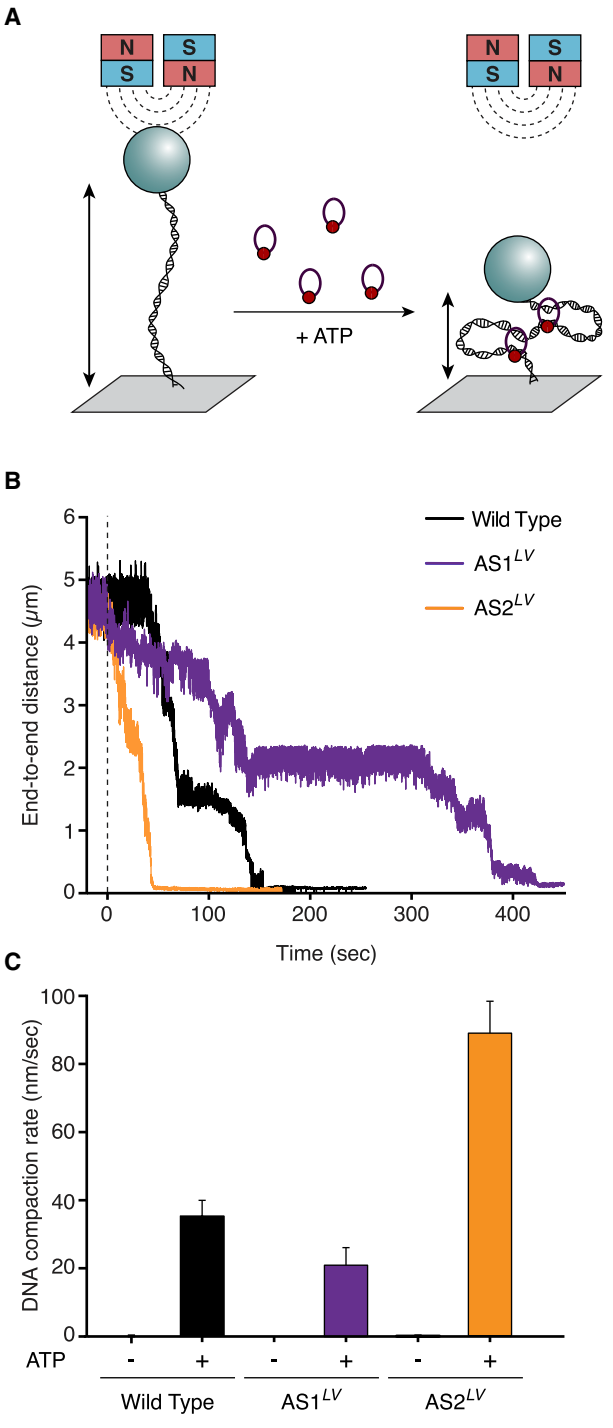

Figure 3. Condensin's ATPase Has Intrinsic Driver and Dampener Sites

(A) Schematic depiction of *in vitro* condensin-mediated DNA compaction using magnetic tweezers.

(B) Representative examples of DNA compaction traces of wild-type, AS1^{LV}, and AS2^{LV}. 10 nM condensin and 1 mM ATP were added at t = 0.

(C) Average DNA compaction rate for wild-type (n = 27), AS1^{LV} (n = 20), and AS2^{LV} (n = 26). The plot shows the mean ± SEM. We used the protein preparations depicted in Figure 4B.

AS1^{LV} mutation had a more pronounced effect than the AS2^{LV} mutation. To assess the consequences of merely reduced condensin levels on the condensation process, we knocked out one *SMC2* allele in a diploid background. Although heterozygous deletion led to a reduction in chromatin-bound condensin that was similar to that observed in AS2^{LV} cells, it resulted in a condensation defect (Figures S2C–S2F). The hyper-condensation phenotype of the AS2^{LV} mutant therefore cannot be explained by simply changing the levels of condensin on mitotic chromosomes.

Because cohesin's release from chromatin is not only dependent on its release factor WAPL, but also on specifically one of cohesin's ATPase sites (Beckouët et al., 2016; Çamdere et al., 2015; Elbatsh et al., 2016; Murayama and Uhlmann, 2015), we studied the effects of the AS1^{LV} and AS2^{LV} mutations on the turnover of condensin I on chromatin by fluorescence recovery after photobleaching (FRAP) experiments (Figures 2C and 2D). Because condensin II is already stably bound to DNA during early mitosis, we did not test whether the turnover of this complex was affected by the AS2^{LV} mutation.

Our FRAP assays fully recapitulated earlier work (Gerlich et al., 2006; Walther et al., 2018), but surprisingly revealed no evident effect of either AS1^{LV} or AS2^{LV} mutations on condensin I turnover. This result is important for a number of reasons. First, it indicates that the hypo- and hyper-condensation phenotypes are not caused by effects on the residence time of condensin I on chromatin. Second, it suggests that condensin's DNA release reaction is regulated differently than cohesin's. This difference may be related to the absence of a WAPL-like release factor in the case of the condensin complex. Finally, because both mutants affect condensin levels on DNA but neither has an effect on its turnover, this indicates that both ATPase sites contribute to the loading of condensin onto DNA.

Hyper-condensed mitotic chromosomes often are a consequence of prolonged mitosis. We therefore followed wild-type and mutant cells through mitosis in real-time (Figure 2E). AS1^{LV} cells took longer than wild-type to progress from NEBD until chromosome alignment in metaphase, and these cells also spent more time between alignment and anaphase onset. Both delays are presumably a consequence of the condensation defects observed in these cells. AS2^{LV} cells, however, progressed through mitosis with normal timing. The observed hyper-condensation effect of the AS2^{LV} mutation therefore cannot be explained by differences in mitotic timing.

Condensin's ATPase Has Intrinsic Driver and Dampener Sites

How then can we explain the opposite condensation phenotypes caused by the AS1^{LV} and AS2^{LV} mutations? An intriguing possibility would be that the two ATPase sites differentially affect the condensation speed. To directly test this hypothesis, we introduced the AS1^{LV} and AS2^{LV} mutations into the *Saccharomyces cerevisiae* condensin complex and used the purified complexes to assess how these mutations affect condensin's DNA compaction activity *in vitro*. We measured the rate of DNA compaction by wild-type and mutant yeast condensin using a recently described magnetic tweezers assay (Figure 3A; Eeftens et al., 2017).

Importantly, this independent *in vitro* system fully recapitulated the *in vivo* results. Complexes harboring the AS1^{LV} mutation compacted DNA at a slower rate than wild-type, whereas condensin complexes with the AS2^{LV} mutation compacted DNA at twice the speed of wild-type (Figures 3B and 3C). We confirmed our results using independent protein preparations (Figure S3A). Our results demonstrate that the AS1^{LV} and AS2^{LV} mutations reciprocally affect condensin's ability to compact DNA, both *in vivo* in human cells and *in vitro* using the budding yeast complexes. This shows that this asymmetric activity is intrinsic to the condensin complex, and also that this function seems to be conserved from yeast to humans. We have hereby identified an unanticipated dual role of condensin's ATPase. AS1 drives mitotic chromosome condensation, while AS2 apparently acts as a dampener whose inactivation results in faster DNA compaction.

ATP Hydrolysis Is Not Rate-Limiting for Loop Enlargement

Recent work shows that condensin can processively enlarge loops in an ATP dose-dependent manner (Ganji et al., 2018). To investigate whether the opposite phenotypes of the AS1^{LV} and AS2^{LV} mutation can be attributed to changes in their ATPase activities, we assessed the effects of these mutations on condensin's ATP hydrolysis *in vitro*. To this end, we used the purified budding yeast complexes to perform ATPase assays using thin-layer chromatography and radiolabeled ATP (Figures 4A and 4B). Consistent with previous work, wild-type condensin efficiently hydrolyzed ATP, which was further stimulated by the addition of DNA (Terakawa et al., 2017). The AS1^{LV} and AS2^{LV} mutations affected hydrolysis to different degrees. Whereas AS1^{LV} mutation reduced both the basic and the DNA-stimulated ATPase activity to about half of that of the wild-type complex, the AS2^{LV} mutation had a very subtle effect on the ATPase activity (Figure 4C). Each ATPase site apparently has a distinct contribution to condensin's ATPase activity. These results suggest that the hypo-condensation phenotype of the AS1^{LV} mutant is presumably due to a reduction in ATP hydrolysis rate that is incompatible with proper chromosome condensation. The hyper-condensation phenotype of the AS2^{LV} condensin mutant is, however, obviously not due to an increase in ATP turnover rates.

To gain detailed insight into how the two ATPase mutants affect DNA loop extrusion, we used a recently developed single-molecule assay (Ganji et al., 2018). This method entails the imaging of a double-stranded DNA that is tethered by its biotinylated ends to a streptavidin-containing surface. The addition of condensin and ATP results in the formation and enlargement of DNA loops that can be visualized by a local and gradual increase in the intensity of the fluorescently labeled DNA (Figure 4D). We used wild-type, AS1^{LV}, or AS2^{LV} mutant budding yeast condensin complexes at low concentration (1 nM condensin) to examine how the individual complexes form loops. Remarkably, AS1^{LV} and AS2^{LV} complexes enlarged loops at the same rate as wild-type condensin (Figures 4E and S4A). This is a surprise, because the AS1^{LV} mutation indeed reduces condensin's ATPase activity by half. Although it is required for loop formation, condensin's ATPase activity thus does not seem to be the rate-limiting step in DNA loop enlargement.

Condensin's ATPase Site 1 Drives Loop Formation

If neither of the ATPase mutants affects DNA loop extrusion rates, then how do these mutants affect the chromosome condensation process? To address whether the AS1^{LV} and AS2^{LV} mutations might be affecting an early step in the process of DNA looping, we measured the fraction of all tethered DNA molecules that displayed a loop. Interestingly, the fraction of DNA that contained at least one loop was strongly reduced in the presence of the AS1^{LV} mutant condensin complexes, whereas the fraction of DNAs with one loop was similar to the wild-type for the AS2^{LV} mutant (Figures 4F, S4A, and S4C). The probability of forming more than one loop on the same DNA molecule was likewise decreased for the AS1^{LV} mutant complexes but was again unaffected by the AS2^{LV} mutation (Figure S4B). These results indicate that the activity of condensin's AS1 plays a vital role in an early step of the loop formation process, but has little effect on the speed of extrusion once a loop has formed. Because condensin has been suggested to depend on its ATPase activity to transit from an unstable, salt-sensitive to a stable, salt-resistant DNA binding mode (Eeftens et al., 2017), it is reasonable to propose that the activity of condensin's AS1 site promotes the topological entrapment of DNA.

Condensin's ATPase Site 2 Promotes the Formation of Higher-Order Z Loop Structures

The AS2^{LV} mutation apparently does not affect condensin's ability to initiate loops, nor does it alter the speed by which it enlarges these loops. How then can we explain that this mutant compacts DNA faster than wild-type not only *in vivo*, but also in the *in vitro* magnetic tweezers set-up? One major difference between the magnetic tweezers and the single-molecule assays is that the former are performed in the presence of a 10-fold higher condensin concentration (10 nM) than the latter (1 nM), where the higher concentration may better mimic the physiological concentration of cellular condensin (Ho et al., 2018; Wang et al., 2005). Although it has been shown that a single condensin can form a DNA loop *in vitro*, higher condensin concentrations may favor the cooperative action of multiple condensin complexes.

We therefore repeated the single-molecule fluorescence-imaging assay using 10 nM wild-type condensin. Intriguingly, we observed that the majority of DNA molecules did not exhibit a single loop, but instead displayed a distinct type of higher-order DNA structure characteristic of a conformation of three DNA strands that were stretched along the DNA and hence result in a broad DNA fluorescence signal (Figure 5A). The detailed analysis of how these "Z loop" structures are formed will be part of a separate study (Kim et al., 2019). To investigate the effect of the AS2^{LV} mutant on these higher-order Z loop structures, we scored their abundance for wild-type and AS2^{LV} mutant complexes. Interestingly, we found considerably fewer (~3 times) higher-order Z loops for the AS2^{LV} mutant (Figures 5B).

We then assessed the stability of higher-order Z loops and found that the disruption of these structures was not affected by the AS2^{LV} mutation. We did note, however, that Z loops in general were significantly (~5 times) more stable once they had formed compared to separate DNA loops (Figure 5C). Condensin thus can form two types of DNA structures: separate DNA loops that are processively enlarged by a single condensin and more stable

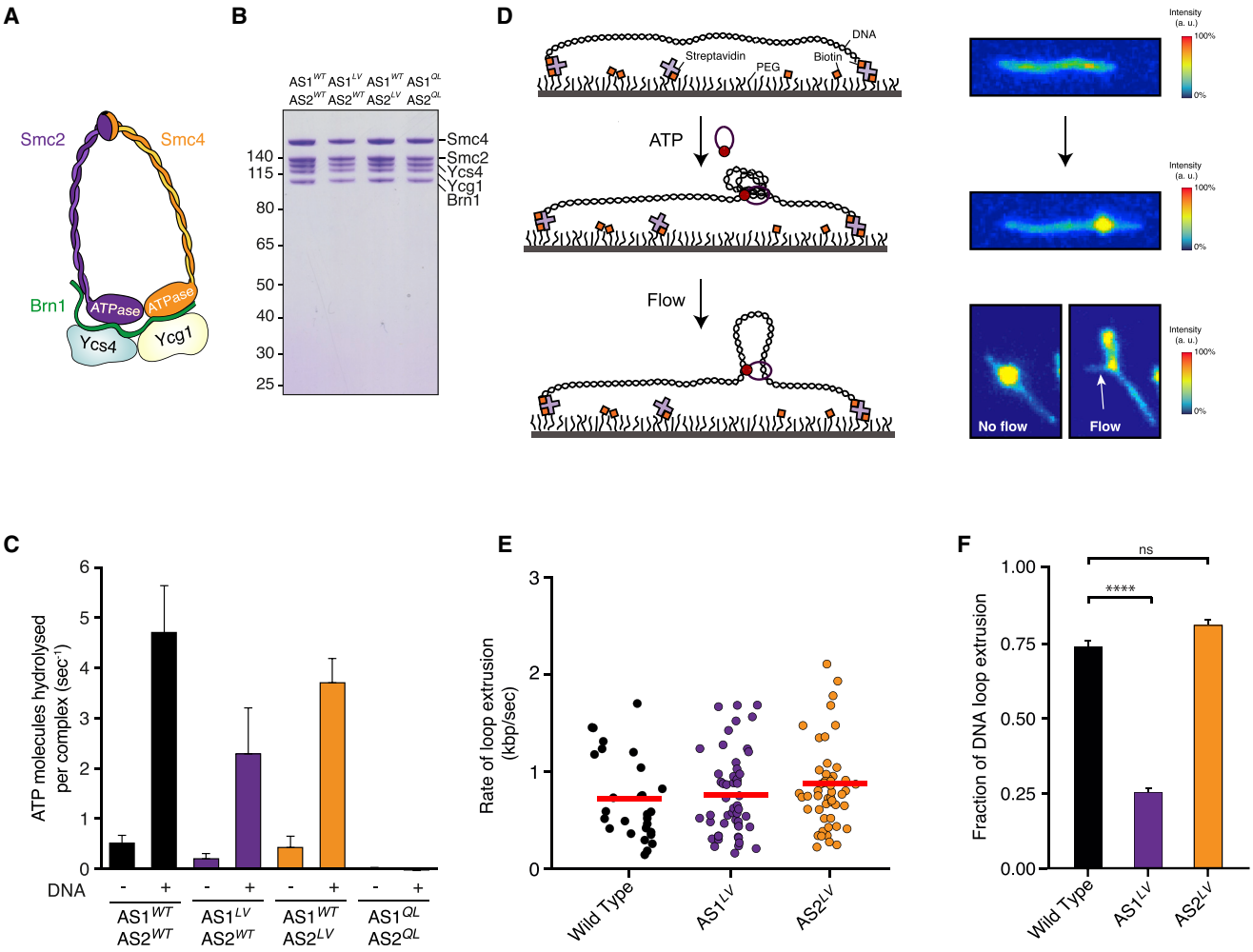

Figure 4. Condensin's ATPase Site 1 Drives Loop Formation

(A) Schematic depiction of the *S. cerevisiae* condensin complex.

(B) Coomassie-stained SDS-PAGE of the condensin holocomplex samples as used in (C).

(C) ATP hydrolysis rates measured for condensin holocomplexes (5 μM) in the absence or presence of 10 μg/μL of a relaxed 6.4-kb plasmid DNA. The graph shows mean ± SD of five independent experiments for wild-type, $AS1^{LV}$ (Smc2 L1048V), and $AS2^{LV}$ (Smc4 L1323V) mutants, and three independent experiments for the negative control, the Q-loop mutant $AS1^{QL}$ (Smc4 Q302L)-$AS2^{QL}$ (Smc2 Q147L).

(D) Schematic overview of single-molecule fluorescence assay for condensin-mediated loop extrusion. DNA is double-tethered to a streptavidin-containing surface and stained with Sytox Orange. The addition of 1 nM condensin and 5 mM ATP results in a loop as judged by the local increase in intensity of the fluorescently labeled DNA. DNA loops can be visualized by applying a flow perpendicular to the tethered DNA molecule.

(E) Rate of DNA loop extrusion by wild-type (n = 27), $AS1^{LV}$ (n = 51), and $AS2^{LV}$ (n = 51) condensin. Each circle represents one DNA molecule. Red line depicts the mean. Only DNA molecules with an extension of <0.65 were included in this graph (for extrusion rates of other DNA extensions check Figure S4A). The experiment was performed using 1 nM condensin and 5 mM ATP.

(F) Fraction of DNA molecules that shows a loop using wild-type (n = 109), $AS1^{LV}$ (n = 237), or $AS2^{LV}$ (n = 124) condensin complexes. The experiment was performed using 1 nM condensin and 5 mM ATP. The graph shows the mean ± 95% confidence interval. Statistical significance was measured using unpaired two-tailed Student's t test, ****p value < 0.0001. ns, non-significant.

higher-order Z loops formed by multiple condensins. Importantly, condensin's ATPase site 2 turns out to promote the formation of these higher-order Z loop structures (Figure 5D).

Condensin's ATPase Site 2 Limits Chromatin Loop Length

The hyper-condensation phenotype observed with the $AS2^{LV}$ mutant could potentially be explained by its relative inability to form higher-order Z loop structures. Processively enlarging loops may indeed condense DNA in a more productive fashion. If the $AS2^{LV}$ mutation does cause hyper-condensation through the favored formation of processively enlarging separate loops, then the average loop length should be longer. To assess loop length, we performed chromosome conformation capture (Hi-C) experiments on mitotic cells. To this end, wild-type or $AS2^{LV}$ mutant mitotic cells were collected by shake-off after a

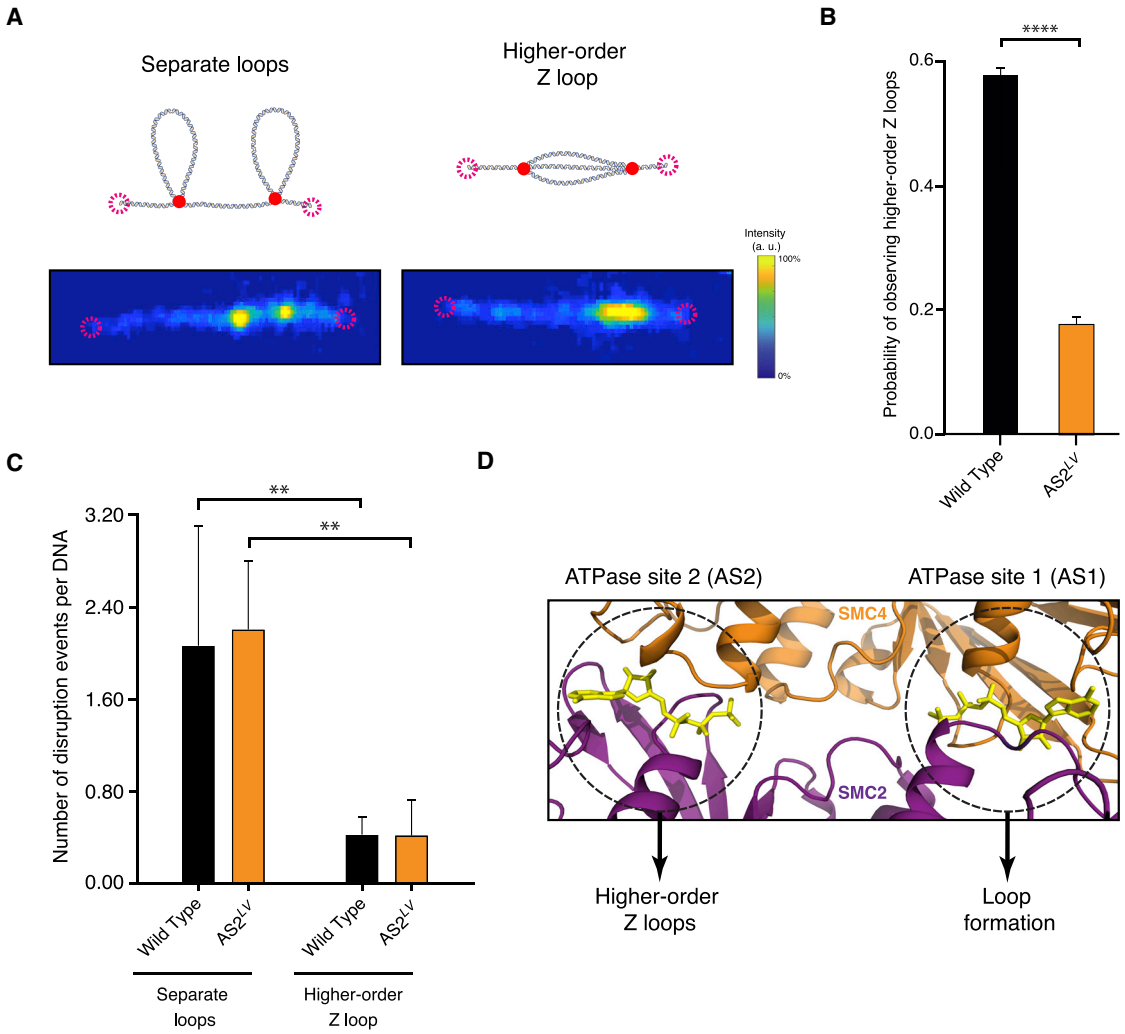

Figure 5. Condensin's ATPase Site 2 Promotes Higher-Order Z Loop Structures

(A) Representative examples of DNA molecules that show separate loops (left) or a higher-order Z loop structure (right). Dotted circles depict tethered ends of the DNA. Above is a schematic for two separate loops (left) or a formed higher-order Z loop structure on one DNA molecule (right). Red circles represent condensin.

(B) Fraction of DNA molecules with higher-order Z loop structures formed by wild-type (n = 189) and AS2^{LV} (n = 199) complexes. The experiment was performed as in Figure 4E, but using 10 nM condensin instead of 1 nM. The graph shows the mean ± 95% confidence interval. Statistical significance was measured using unpaired two-tailed Student's t test, ****p value < 0.0001.

(C) Number of disruption events per DNA molecule for separate loops and higher-order Z loop structures formed by wild-type and AS2^{LV} complexes during the course of imaging (10 min). The plots show the mean ± SD. Statistical significance was measured using unpaired two-tailed Student's t test, **p value < 0.0017.

(D) A model depicting the dual role of condensin's ATPase in chromosome condensation. Condensin's ATPase machinery contains two ATPase sites. We propose that these two sites have distinct roles in chromosome condensation. AS1 drives condensation by promoting DNA loop formation. AS2 is involved in the formation of less-productive but more stable higher-order Z loop structures. The balanced activity of AS1 and AS2 is key to chromosome condensation.

brief treatment with the microtubule poison nocodazole. These cells were crosslinked with formaldehyde, stained with a mitosis-specific antibody, and then isolated by fluorescence-activated cell sorting (FACS). This protocol resulted in a pure population of mitotic cells that was then processed for Hi-C (Figure S5).

Wild-type cells, in correspondence with earlier work (Naumova et al., 2013), yielded a Hi-C map with homogeneous interactions along the whole lengths of chromosomes. This uniform interaction pattern consisted of a band enriched for *cis*-contacts up to distances of ~12 Mb away from the main diagonal (Figures 6A and S6A). AS2^{LV} mutant cells instead displayed a band of *cis*-contacts that increased to ~25 Mb (Figures 6A, 6B, and S6A). This increase in contact length would be in correspondence with the formation of larger chromatin loops by hyperactive AS2^{LV} condensin. Together, these results would therefore support the model that hyperactive AS2^{LV} condensin results in shorter chromosomes by favoring the formation of these more productive loops.

Together, condensin's AS2 could thus act as a dampener of chromosome condensation by promoting the formation of less-productive higher-order Z loop structures, which limit the

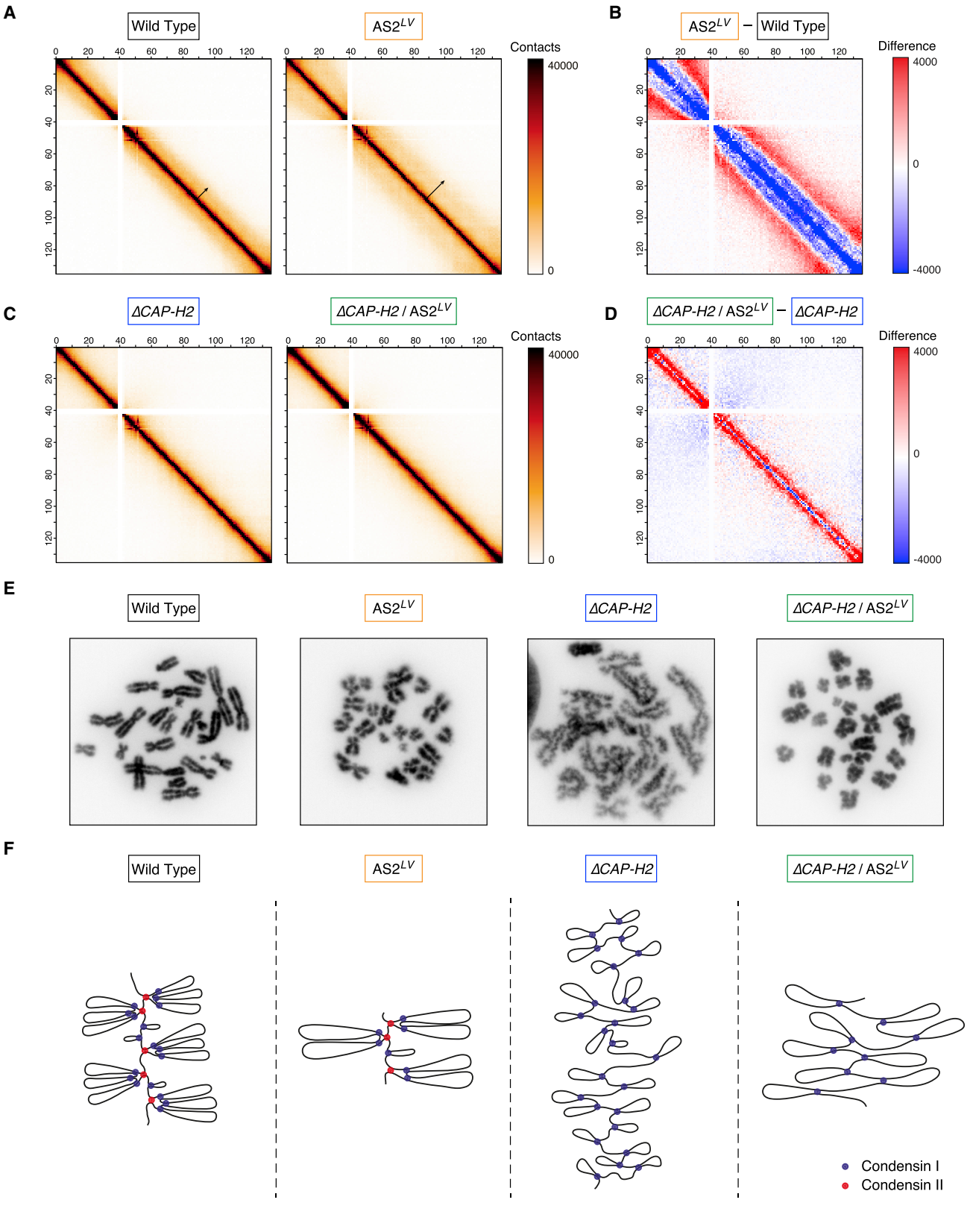

(legend on next page)

degree to which chromatin loops can be enlarged. Provided that there is enough DNA between the individual condensin complexes to keep extruding, a preference for productive separate loops could well lead to hyper-condensed chromosomes. Notably, the AS2^{LV} mutation also reduces condensin levels on chromatin, which provides the necessary space between adjacent condensin complexes for further reeling of DNA that ultimately results in greater loop enlargement.

Hyperactive Condensin I Shortens Chromosomes in the Total Absence of Condensin II

Metazoans express two distinct condensin complexes. The difference in the localization, stability, and levels on chromatin between condensin I and condensin II hints at specific roles for each of the two complexes. Moreover, whereas condensin I is key to lateral chromosome compaction, condensin II is thought to be specifically required for the shortening of chromosomes (Green et al., 2012; Shintomi and Hirano, 2011). Recent super-resolution imaging and Hi-C experiments on mitotic chromosomes suggest that these two complexes shape mitotic chromosomes by forming loops with different sizes (Gibcus et al., 2018; Walther et al., 2018). These studies propose that condensin II is required to build long chromatin loops, while condensin I is responsible for the formation of smaller loops within the larger condensin II-mediated loops.

Because condensin I and II share the same SMC subunits, the AS1^{LV} and AS2^{LV} mutations affect both complexes (Figure 1A). Our ability to hyper-activate condensin I with the AS2^{LV} mutation allowed us to test whether condensin II has an irreplaceable role in structuring mitotic chromosomes. We first knocked out the condensin II-specific subunit CAP-H2 in HAP1 cells using CRISPR/Cas9 (Figure S6B). As expected, *ΔCAP-H2* cells displayed condensation defects that ranged in severity from cells with long and zig-zag shaped chromosomes to others with an indiscernible fuzzy chromatin mass (Figures 6E and S6C). *ΔCAPH-2* cells also exhibited chromosome segregation errors and were delayed in mitosis (Figures 7A and S6D). We then examined which *ΔCAP-H2* defects can or cannot be rescued by hyper-activating condensin I with the AS2^{LV} mutation. We therefore introduced this mutation into *ΔCAP-H2* HAP1 cells (Figure S7A). It is worth noting that we were unable to obtain cells with the AS1^{LV} mutation in a *ΔCAP-H2* background. Because each individual mutation results in condensation and segregation defects, this specific combination presumably is synthetic lethal (Figures S7B and S7D).

Interestingly, chromosomes of *ΔCAP-H2* cells expressing the hyper-activating AS2^{LV} mutant condensed their chromosomes into structures that were generally even shorter than wild-type chromosomes (Figure 6E). The hyper-activating AS2^{LV} mutation also rescued the high percentage of fuzzy chromosomes caused by condensin II deficiency (Figure S7B). Notably, condensin I turnover was affected neither by condensin II deficiency nor by the AS2^{LV} mutation (Figure S7C). Stably chromosome-bound condensin II, therefore, is neither inherently required for efficient condensation nor for the shortening of chromosomes in particular. However, upon closer examination of the hyper-condensed chromosomes, we noticed that chromosomes of *ΔCAP-H2* cells harboring the hyper-activating AS2^{LV} mutant appeared less straight than those of AS2^{LV} single mutant cells (Figures 6E and 6F).

We then compared the Hi-C profiles of *ΔCAP-H2* cells and *ΔCAP-H2* cells with the AS2^{LV} mutation. *ΔCAP-H2* cells lost their long-range interactions when compared to wild-type cells, in correspondence with a requirement for condensin II in forming large DNA loops (Figure S6E). The *ΔCAP-H2* cells with the AS2^{LV} mutation did not regain the long-range contacts in the 12–25 Mb range (Figure 6C). How then can the AS2^{LV} mutant yield hyper-condensed chromosomes both in wild-type and in *ΔCAP-H2* cells, if their interaction maps are so different? To address this question, we plotted the difference in interactions between the respective genotypes (Figure 6D). We found that the AS2^{LV} mutant in *ΔCAP-H2* cells in fact did display an increase in longer-range contacts that shifted from very short-range contacts close to the diagonal of the Hi-C map to contacts of up to ~5 Mb distances. This suggests that condensin I when hyper-activated generates extended loops that are sufficient to shorten mitotic chromosomes.

Taken together, condensin I and II each form loops with specific ranges in size. Condensin II forms long loops, while condensin I forms smaller loops. Hyper-activation of either of these complexes by the AS2^{LV} mutation appears to yield extended loops within the size-range of the respective complex. Even though the AS2^{LV} mutant yields hyper-condensed chromosomes both in wild-type and in *ΔCAP-H2* cells and chromosomes superficially look similar, condensin II does have a specific role in the organization of these chromosomes. We propose that the formation of condensin II-specific long loops is required for a straight chromosomal axis (Figure 6F).

Condensin II Specifically Prevents the Formation of Ultrafine Bridges

Proper condensation is a prerequisite for faithful chromosome segregation (Gerlich et al., 2006; Nagasaka et al., 2016). Consistently, *ΔCAP-H2* cells suffer from an increase in chromosome

Figure 6. Hyper-Active Condensin I Shortens Mitotic Chromosomes in the Total Absence of Condensin II

(A) Whole-chromosome Hi-C matrices of mitotic cells. Cells were harvested by mitotic shake-off after 1.5 h nocodazole treatment. The harvested cells were further selected for their mitotic status by FACS for phospho-MPM2 positivity (see Figure S5 for details). Chromosome 10 is shown at 1 Mb resolution. Arrows depict the distance of contacts in wild-type (up to ~12 Mb) and in AS2^{LV} mutant cells (up to ~25 Mb).

(B) Differential Hi-C signal between the indicated cell lines.

(C) Whole-chromosome Hi-C matrices of mitotic cells of the indicated cell lines. Cells were prepared as in (A).

(D) Differential Hi-C signal between the indicated cell lines.

(E) Representative examples of chromosome spreads of the indicated cell lines. At least 120 spreads were examined in three independent experiments.

(F) Schematic depiction of mitotic chromosome structure in the indicated genotypes. Condensin I complexes are depicted as blue circles and condensin II as red circles.

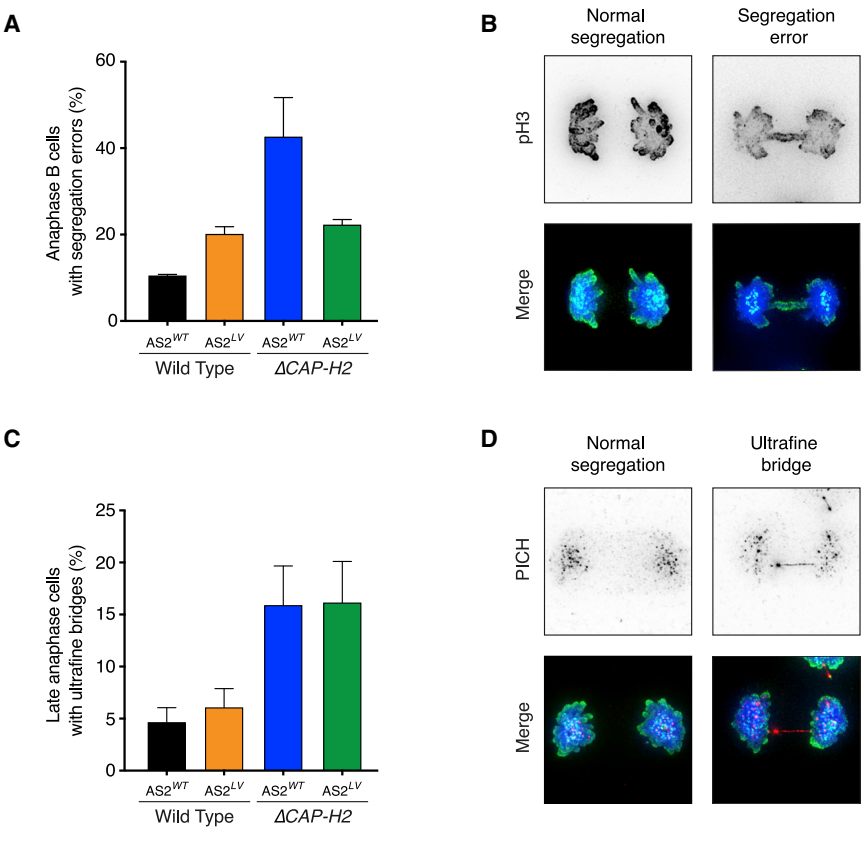

Figure 7. Condensin II Specifically Prevents the Formation of Ultrafine Bridges

(A) Quantification of segregation errors that occur during anaphase for the indicated cell lines. The plot shows the mean ± SD of three independent experiments, with at least 50 anaphases per experiment.

(B) Representative anaphases with either normal segregation or a missegregation as quantified in (A). DNA was visualized by immunofluorescence with DAPI staining (blue), phosphorylated histone H3 (pH3) (green), and centromeres were visualized by CREST (cyan).

(C) Quantification of ultrafine bridges (UFBs), as visualized by PICH staining, in late anaphase cells (anaphase B). The plot shows the mean ± SD of three independent experiments, with at least 50 anaphases per experiment. See Figure S7G to compare to UFBs of early anaphase cells (anaphase A).

(D) Representative anaphases with normal segregation or an ultrafine bridge (UFB) as quantified in (C). DNA was visualized by immunofluorescence with DAPI staining (blue), UFBs by PICH staining (red), and centromeres were visualized by CREST (cyan).

(E) Schematic model of the specific roles of condensin I and II in structuring chromosomes. Both condensin II and hyperactive condensin I (condensin I AS2^{LV}) can shorten mitotic chromosomes. Only condensin II plays a specific role in the decatenation of entangled DNAs from S phase onward. Cohesin complexes connecting the sister chromatids are depicted in green.

segregation errors compared to wild-type cells (Figures 7A and 7B). In correspondence with the rescue of the major condensation defect, the hyper-activating AS2^{LV} mutant also largely rescued this segregation defect (Figures 7A and 7B). AS2^{LV} mutant cells and *ΔCAPH2* cells harboring AS2^{LV} both displayed the same degree of basic segregation errors. However, neither of these genotypes displayed wild-type like segregation fidelity. This indicates that hyper-condensation may not be beneficial for faithful chromosome segregation.

Mitoses of *ΔCAP-H2* cells also displayed an increase in ultrafine bridges (Figures 7C, 7D, and S7F–S7H). This is interesting, because condensin II is nuclear throughout the cell cycle and plays a role in the resolution of sister chromatids from S phase onward (Ono et al., 2013; Piskadlo et al., 2017). This resolution could, for example, aid the disentangling or decatenation of sister DNAs. The persistence of such catenanes can lead to ultrafine DNA bridges during mitosis. Condensin I only contacts DNA upon nuclear envelope breakdown (NEBD). Importantly, we find that hyperactive condensin I cannot rescue the increase in ultrafine bridges observed in *ΔCAP-H2* cells. Together, this would support the model that hyperactive condensin I by itself can condense chromosomes within the relatively short window spanning the time from NEBD to metaphase, but that the decatenation of entangled DNAs requires more time and therefore needs the presence of condensin II from S phase onward (Figure 7E).

DISCUSSION

Condensin's Two ATPase Sites Play Distinct Roles

How condensin's ATPase drives mitotic chromosome condensation is a major question of chromosome biology. We here identify an unexpected dual role for this machinery that is conserved from yeast to humans. Specifically one of condensin's ATPase sites (AS1) drives loop formation, while the other ATPase site (AS2) promotes the formation of higher-order Z loop structures

(Figure 5D). Because SMC complexes organize genomes from bacteria to humans, we suggest that such an asymmetric division of tasks may reflect a universal principle for these molecular motors.

Cohesin's ATPase machinery also harbors an asymmetric activity, which is evident from the fact that only one of cohesin's ATPase sites is required for cohesin release from DNA. Our FRAP experiments, however, indicate that the analogous ATPase site in condensin (AS2) does not play such a role. This might well be related to the fact that condensin has no dedicated WAPL-like release factor. How condensin in fact releases DNA remains unclear. It is striking though that the analogous site in both cases has a function that is antagonistic to the overall function of the complex. For condensin, this site has a dampening function, while for cohesin it is required for the release of this complex from chromatin. Condensin's HEAT-repeat subunits have contrasting functions in condensation (Kinoshita et al., 2015; Lavoie et al., 2002). Whether these opposing functions are linked to the ATPase machinery is yet unknown. Each of these proteins binds to a different part of condensin's kleisin subunit (Onn et al., 2007; Piazza et al., 2014). Moreover, recent work on the *E. coli* SMC complex, MukBEF, indicates that the individual ATPase sites can be regulated independently through binding to different parts of the kleisin (Zawadzka et al., 2018).

Recent single-molecule experiments have shown that condensin is a molecular motor that can processively enlarge loops in an ATP-dependent manner (Ganji et al., 2018). ATP hydrolysis is required both for condensin's stable, salt-resistant DNA binding and for subsequent compaction of DNA (Eeftens et al., 2017; Strick et al., 2004). Hydrolysis-deficient condensin complexes were previously found to localize to chromatin (Hudson et al., 2008; Kinoshita et al., 2015; Palou et al., 2018; Thadani et al., 2018), but considering the available *in vitro* data, these complexes presumably were not stably bound to DNA. This is in line with experiments using these classical "Walker B" mutant forms of the cohesin complex (Hu et al., 2011; Ladurner et al., 2014). Intriguingly, the $AS1^{LV}$ and $AS2^{LV}$ mutants are partially impaired in their ATPase activity, but they do bind DNA with wild-type like stability *in vivo* as judged by FRAP. The analogous mutations in the cohesin complex are proficient in ATP binding and ADP release, and display reduced ATP hydrolysis (Elbatsh et al., 2016). Reduced ATP hydrolysis is unlikely to be the explanation of the hyper-condensation phenotype observed for the $AS2^{LV}$ mutant. We therefore suggest that this signature motif mutation affects a key conformational change in the complex that would normally limit the degree of condensation. The partial inactivation of condensin's ATPase cycle has allowed us to investigate the roles of the different ATPase sites post condensin loading. We propose that both sites are involved in loading, but that specifically AS1 is important for the condensation process itself, which in turn is dampened by AS2.

AS1 and AS2: The Engine's Start and Stop Buttons

We find that the ATPase activity of condensin is surprisingly not rate-limiting for the loop enlargement process itself. Despite reduced ATP hydrolysis, the $AS1^{LV}$ mutant does not affect the speed of loop enlargement, but rather impairs loop formation. This is in accordance with recent findings in *B. subtilis* that impairing the ATPase activity of the SMC complex in this species delays loop formation (Wang et al., 2018). Interestingly, a very recent study shows that ATP binding by the Smc2 and Smc4 ATPase heads has distinct consequences for the architecture of the condensin complex. Whereas the latter can initiate ATP binding in the absence of its partner, the nucleotide binding by the former can only take place once the head heterodimer has been formed (Hassler et al., 2019). This result would be in agreement with our finding that specifically AS1 initiates condensation. How does the driver ATPase site (AS1) then control this step of loop formation? We suggest that AS1 either promotes the entrapment of a second DNA element within condensin's lumen to form an initial tiny loop, or that it kick-starts the loop enlargement process. Both these steps are likely to require a drastic conformational change in the complex's structure that could involve specifically this ATPase site.

Mutation of AS2 results in hyper-condensation without affecting mitotic timing, condensin's turnover on chromatin, or increasing ATP hydrolysis rates. Instead, mutating this site drastically diminishes the formation of higher-order Z loop structures. How could this then lead to the hyper-condensation phenotype? We suggest that this could be related to a fundamental difference between separate loops and Z loops. Two condensin complexes that are each forming a separate loop can in essence keep processively enlarging their loops, provided that they encounter no obstacles. Two condensin complexes that together form a Z loop can, however, only shorten a given DNA segment up to a maximum of 3-fold (Kim et al., 2019). A preference of the $AS2^{LV}$ mutant for separate loops over Z loops could therefore lead to shorter, hyper-condensed, chromosomes.

But why would wild-type condensin actually form such Z loops if this limits the degree of condensation? Would it not be beneficial for cells to be able to condense DNA more efficiently? One possibility is that cells may want to restrict the length of chromatin loops. This could, for example, prevent DNA entanglements between sister chromatids. This model is supported by our finding that $AS2^{LV}$ mutant cells, which harbor longer DNA loops, also show an increase in chromatin bridges. By preventing the formation of long loops, AS2 would hereby ensure faithful chromosome segregation. AS2-dependent higher-order Z loops could also serve to stabilize chromatin loops. In line with this possibility, these structures indeed are more stable than separate loops.

Condensin I versus Condensin II

Metazoans have two distinct condensin complexes that differ in their protein composition, cellular localization, abundance, and stability on DNA. We find that condensin II-deficient cells have long and fuzzy chromosomes, but that hyperactive condensin I can efficiently shorten chromosomes even in the total absence of condensin II. This is surprising, because condensin II is thought to have a specific role in the shortening of mitotic chromosomes (Shintomi and Hirano, 2011). We propose that the time from NEBD to anaphase is not sufficient for wild-type condensin I to condense chromosomes without the help of condensin II, but condensin II does not have an irreplaceable function in this process.

We find that condensin II does have at least two key roles that cannot be compensated for by hyper-active condensin I. The first is that condensin II has a specific role in the formation of longer-range *cis* contacts than does condensin I. Considering these findings and the timing at which the two complexes contact DNA, our data would support the hypothesis that condensin II initiates condensation by forming long loops and that, upon NEBD, condensin I makes small loops within these larger loops (Figure S7I). This is also consistent with earlier work showing that condensin I is important for reducing the width of chromosomes (Shintomi and Hirano, 2011). Condensin II in a normal setting would then be important for the shortening of chromosomes, but we find that this role can be taken over by hyperactive condensin I.

A recent study proposed that condensin II plays a role in the formation of a helical turn within the axis of mitotic chromosomes and that the megabase-scale contacts measured in these experiments reflect interactions between loops that are stacked in a helical fashion (Gibcus et al., 2018). We find that mitotic chromosomes can efficiently be shortened without such a condensin II-dependent helical axis. Notably, these shortened chromosomes are morphologically distinct because they appear less straight. The condensin II-specific long loops therefore might be important for the formation of straight chromosomes.

We suggest that specifically condensin II plays a key role in the decatenation of sister chromatids. The nuclear localization of condensin II may allow this complex to aid decatenation from S phase onward. Even though hyperactive condensin I is sufficient for the condensation process per se within the limited time window from NEBD to anaphase, the decatenation process may well require considerably more time and might mostly take place during interphase. Condensin I can in fact regulate DNA catenation, because its inactivation in *Drosophila* cells during metaphase results in an increase in catenanes (Piskadlo et al., 2017). We therefore expect that condensin II's contribution to decatenation simply is a consequence of the spatiotemporal regulation of this complex.

Hyper-activation of both condensin I and condensin II leads to hyper-condensed chromosomes, but interestingly this also causes an increase in chromosome segregation errors. This indicates that condensin's ability to condense chromosomes needs dampening to ensure faithful chromosome segregation. The balanced activity of the two ATPase sites indeed appears to be key to both the condensation and the segregation of chromosomes. We propose that asymmetric ATPases with distinct roles for each ATPase site reflect a universal principle that enables the ancient family of SMC protein complexes to intricately control chromosome architecture.

STAR★METHODS

Detailed methods are provided in the online version of this paper and include the following:

- KEY RESOURCES TABLE
- LEAD CONTACT AND MATERIALS AVAILABILITY
- EXPERIMENTAL MODEL AND SUBJECT DETAILS
  - Cell line
- METHOD DETAILS
  - Genome Editing
  - ATPase Assays
  - Structural Model
  - Immunofluorescence
  - Magnetic Tweezers
  - Single-Molecule Fluorescence Assay
  - Hi-C
  - Chromosome Spreads
  - Live-Cell Imaging
  - Fluorescence Recovery After Photobleaching (FRAP) Assays
  - Western Blotting
- QUANTIFICATION AND STATISTICAL ANALYSIS
- DATA AND CODE AVAILABILITY

SUPPLEMENTAL INFORMATION

Supplemental Information can be found online at https://doi.org/10.1016/j.molcel.2019.09.020.

ACKNOWLEDGMENTS

We are grateful to all members of the Rowland and Medema Laboratories for helpful discussions, Tatsuya Hirano for the CAPH2 antibody, Roy van Heesbeen, Martijn van Baalen and Jacob Kerssemakers for technical assistance, Ana Kalichava for contributing to early experiments, Bram van den Broek for advice on imaging, and the NKI protein production, Microscopy, and FACS facilities for assistance. We thank Titia Sixma and Kim Nasmyth for discussions and Martin Houlard for imaging in murine cells. We acknowledge the Netherlands Organisation for Scientific Research (NWO ECHO), the Dutch Cancer Society (KWF), and the European Research Council (ERC) for funding.

AUTHOR CONTRIBUTIONS

A.M.O.E., A.G.-N., and J.u.d.B. performed cell biology experiments. E.K. and M.G. performed single-molecule fluorescence experiments. J.M.E. performed magnetic tweezer experiments. A.M.O.E. and J.A.R. generated cell lines. S.B. and C.H.H. purified recombinant condensin complexes and performed ATPase assays. A.M.O.E. and H.T. prepared Hi-C samples and R.H.v.d.W. and E.d.W. analyzed Hi-C data. A.M.O.E. and B.D.R. wrote the manuscript with input from all authors.

DECLARATION OF INTERESTS

The authors declare no competing interests.

Received: March 12, 2019
Revised: July 17, 2019
Accepted: September 13, 2019
Published: October 16, 2019

REFERENCES

Beckouët, F., Srinivasan, M., Roig, M.B., Chan, K.L., Scheinost, J.C., Batty, P., Hu, B., Petela, N., Gligoris, T., Smith, A.C., et al. (2016). Releasing Activity Disengages Cohesin's Smc3/Scc1 Interface in a Process Blocked by Acetylation. Mol. Cell *61*, 563–574.

Blomen, V.A., Májek, P., Jae, L.T., Bigenzahn, J.W., Nieuwenhuis, J., Staring, J., Sacco, R., van Diemen, F.R., Olk, N., Stukalov, A., et al. (2015). Gene essentiality and synthetic lethality in haploid human cells. Science *350*, 1092–1096.

Çamdere, G., Guacci, V., Stricklin, J., and Koshland, D. (2015). The ATPases of cohesin interface with regulators to modulate cohesin-mediated DNA tethering. eLife *4*, 1–66.

Carette, J.E., Raaben, M., Wong, A.C., Herbert, A.S., Obernosterer, G., Mulherkar, N., Kuehne, A.I., Kranzusch, P.J., Griffin, A.M., Ruthel, G., et al. (2011). Ebola virus entry requires the cholesterol transporter Niemann-Pick C1. Nature *477*, 340–343.

Cuylen, S., Metz, J., and Haering, C.H. (2011). Condensin structures chromosomal DNA through topological links. Nat. Struct. Mol. Biol. *18*, 894–901.

Eeftens, J.M., Bisht, S., Kerssemakers, J., Kschonsak, M., Haering, C.H., and Dekker, C. (2017). Real-time detection of condensin-driven DNA compaction reveals a multistep binding mechanism. EMBO J. *36*, 3448–3457.

Elbatsh, A.M.O., Haarhuis, J.H.I., Petela, N., Chapard, C., Fish, A., Celie, P.H., Stadnik, M., Ristic, D., Wyman, C., Medema, R.H., et al. (2016). Cohesin Releases DNA through Asymmetric ATPase-Driven Ring Opening. Mol. Cell *61*, 575–588.

Ganji, M., Shaltiel, I.A., Bisht, S., Kim, E., Kalichava, A., Haering, C.H., and Dekker, C. (2018). Real-time imaging of DNA loop extrusion by condensin. Science *360*, 102–105.

Gerlich, D., Hirota, T., Koch, B., Peters, J.-M., and Ellenberg, J. (2006). Condensin I stabilizes chromosomes mechanically through a dynamic interaction in live cells. Curr. Biol. *16*, 333–344.

Gibcus, J.H., Samejima, K., Goloborodko, A., Samejima, I., Naumova, N., Nuebler, J., Kanemaki, M.T., Xie, L., Paulson, J.R., Earnshaw, W.C., et al. (2018). A pathway for mitotic chromosome formation. Science *359*, eaao6135.

Green, L.C., Kalitsis, P., Chang, T.M., Cipetic, M., Kim, J.H., Marshall, O., Turnbull, L., Whitchurch, C.B., Vagnarelli, P., Samejima, K., et al. (2012). Contrasting roles of condensin I and condensin II in mitotic chromosome formation. J. Cell Sci. *125*, 1591–1604.

Haarhuis, J.H.I., van der Weide, R.H., Blomen, V.A., Yáñez-Cuna, J.O., Amendola, M., van Ruiten, M.S., Krijger, P.H.L., Teunissen, H., Medema, R.H., van Steensel, B., et al. (2017). The Cohesin Release Factor WAPL Restricts Chromatin Loop Extension. Cell *169*, 693–707.

Haering, C.H., and Gruber, S. (2016). SnapShot: SMC Protein Complexes Part I. Cell *164*, 326–326.

Hassler, M., Shaltiel, I.A., and Haering, C.H. (2018). Towards a Unified Model of SMC Complex Function. Curr. Biol. *28*, R1266–R1281.

Hassler, M., Shaltiel, I.A., Kschonsak, M., Simon, B., Merkel, F., Thärichen, L., Bailey, H.J., Macošek, J., Bravo, S., Metz, J., et al. (2019). Structural Basis of an Asymmetric Condensin ATPase Cycle. Mol. Cell *74*, 1175–1188.

Hirano, T. (2012). Condensins: universal organizers of chromosomes with diverse functions. Genes Dev. *26*, 1659–1678.

Hirano, T. (2016). Condensin-Based Chromosome Organization from Bacteria to Vertebrates. Cell *164*, 847–857.

Hirano, T., and Mitchison, T.J. (1994). A heterodimeric coiled-coil protein required for mitotic chromosome condensation in vitro. Cell *79*, 449–458.

Hirota, T., Gerlich, D., Koch, B., Ellenberg, J., and Peters, J.-M. (2004). Distinct functions of condensin I and II in mitotic chromosome assembly. J. Cell Sci. *117*, 6435–6445.

Ho, B., Baryshnikova, A., and Brown, G.W. (2018). Unification of Protein Abundance Datasets Yields a Quantitative Saccharomyces cerevisiae Proteome. Cell Syst. *6*, 192–205.

Hopfner, K.-P. (2016). Invited review: Architectures and mechanisms of ATP binding cassette proteins. Biopolymers *105*, 492–504.

Hu, B., Itoh, T., Mishra, A., Katoh, Y., Chan, K.L., Upcher, W., Godlee, C., Roig, M.B., Shirahige, K., and Nasmyth, K. (2011). ATP hydrolysis is required for relocating cohesin from sites occupied by its Scc2/4 loading complex. Curr. Biol. *21*, 12–24.

Hudson, D.F., Ohta, S., Freisinger, T., Macisaac, F., Sennels, L., Alves, F., Lai, F., Kerr, A., Rappsilber, J., and Earnshaw, W.C. (2008). Molecular and genetic analysis of condensin function in vertebrate cells. Mol. Biol. Cell *19*, 3070–3079.

Kim, E., Kerssemakers, J., Shantiel, I.A., Haering, C.H., and Dekker, C. (2019). DNA-loop extruding condensin complexes can traverse one another. bioRxiv. https://doi.org/10.1101/682864.

Kinoshita, K., Kobayashi, T.J., and Hirano, T. (2015). Balancing acts of two HEAT subunits of condensin I support dynamic assembly of chromosome axes. Dev. Cell *33*, 94–106.

Kschonsak, M., Merkel, F., Bisht, S., Metz, J., Rybin, V., Hassler, M., and Haering, C.H. (2017). Structural Basis for a Safety-Belt Mechanism That Anchors Condensin to Chromosomes. Cell *171*, 588–600.e24.

Ladurner, R., Bhaskara, V., Huis in 't Veld, P.J., Davidson, I.F., Kreidl, E., Petzold, G., and Peters, J.-M. (2014). Cohesin's ATPase activity couples cohesin loading onto DNA with Smc3 acetylation. Curr. Biol. *24*, 2228–2237.

Lavoie, B.D., Hogan, E., and Koshland, D. (2002). In vivo dissection of the chromosome condensation machinery: reversibility of condensation distinguishes contributions of condensin and cohesin. J. Cell Biol. *156*, 805–815.

Murayama, Y., and Uhlmann, F. (2015). DNA Entry into and Exit out of the Cohesin Ring by an Interlocking Gate Mechanism. Cell *163*, 1628–1640.

Nagasaka, K., Hossain, M.J., Roberti, M.J., Ellenberg, J., and Hirota, T. (2016). Sister chromatid resolution is an intrinsic part of chromosome organization in prophase. Nat. Cell Biol. *18*, 692–699.

Nasmyth, K., and Haering, C.H. (2005). The structure and function of SMC and kleisin complexes. Annu. Rev. Biochem. *74*, 595–648.

Naumova, N., Imakaev, M., Fudenberg, G., Zhan, Y., Lajoie, B.R., Mirny, L.A., and Dekker, J. (2013). Organization of the mitotic chromosome. Science *342*, 948–953.

Nishide, K., and Hirano, T. (2014). Overlapping and non-overlapping functions of condensins I and II in neural stem cell divisions. PLoS Genet. *10*, e1004847.

Onn, I., Aono, N., Hirano, M., and Hirano, T. (2007). Reconstitution and subunit geometry of human condensin complexes. EMBO J. *26*, 1024–1034.

Ono, T., Losada, A., Hirano, M., Myers, M.P., Neuwald, A.F., and Hirano, T. (2003). Differential contributions of condensin I and condensin II to mitotic chromosome architecture in vertebrate cells. Cell *115*, 109–121.

Ono, T., Yamashita, D., and Hirano, T. (2013). Condensin II initiates sister chromatid resolution during S phase. J. Cell Biol. *200*, 429–441.

Palou, R., Dhanaraman, T., Marrakchi, R., Pascariu, M., Tyers, M., and D'Amours, D. (2018). Condensin ATPase motifs contribute differentially to the maintenance of chromosome morphology and genome stability. PLoS Biol. *16*, e2003980.

Piazza, I., Rutkowska, A., Ori, A., Walczak, M., Metz, J., Pelechano, V., Beck, M., and Haering, C.H. (2014). Association of condensin with chromosomes depends on DNA binding by its HEAT-repeat subunits. Nat. Struct. Mol. Biol. *21*, 560–568.

Piskadlo, E., Tavares, A., and Oliveira, R.A. (2017). Metaphase chromosome structure is dynamically maintained by condensin I-directed DNA (de)catenation. eLife *6*, e26120.

Saitoh, N., Goldberg, I.G., Wood, E.R., and Earnshaw, W.C. (1994). ScII: an abundant chromosome scaffold protein is a member of a family of putative ATPases with an unusual predicted tertiary structure. J. Cell Biol. *127*, 303–318.

Servant, N., Varoquaux, N., Lajoie, B.R., Viara, E., Chen, C.-J., Vert, J.-P., Heard, E., Dekker, J., and Barillot, E. (2015). HiC-Pro: an optimized and flexible pipeline for Hi-C data processing. Genome Biol. *16*, 259.

Shintomi, K., and Hirano, T. (2011). The relative ratio of condensin I to II determines chromosome shapes. Genes Dev. *25*, 1464–1469.

Strick, T.R., Kawaguchi, T., and Hirano, T. (2004). Real-time detection of single-molecule DNA compaction by condensin I. Curr. Biol. *14*, 874–880.

Strunnikov, A.V., Hogan, E., and Koshland, D. (1995). SMC2, a Saccharomyces cerevisiae gene essential for chromosome segregation and condensation, defines a subgroup within the SMC family. Genes Dev. *9*, 587–599.

Terakawa, T., Bisht, S., Eeftens, J.M., Dekker, C., Haering, C.H., and Greene, E.C. (2017). The condensin complex is a mechanochemical motor that translocates along DNA. Science *358*, 672–676.

Thadani, R., Kamenz, J., Heeger, S., Muñoz, S., and Uhlmann, F. (2018). Cell-Cycle Regulation of Dynamic Chromosome Association of the Condensin Complex. Cell Rep. *23*, 2308–2317.

Uhlmann, F. (2016). SMC complexes: from DNA to chromosomes. Nat. Rev. Mol. Cell Biol. *17*, 399–412.

van Ruiten, M.S., and Rowland, B.D. (2018). SMC Complexes: Universal DNA Looping Machines with Distinct Regulators. Trends Genet. *34*, 477–487.

Vian, L., Pękowska, A., Rao, S.S.P., Kieffer-Kwon, K.-R., Jung, S., Baranello, L., Huang, S.-C., El Khattabi, L., Dose, M., Pruett, N., et al. (2018). The Energetics and Physiological Impact of Cohesin Extrusion. Cell *173*, 1165–1178.e20.

Walther, N., Hossain, M.J., Politi, A.Z., Koch, B., Kueblbeck, M., Ødegård-Fougner, Ø., Lampe, M., and Ellenberg, J. (2018). A quantitative map of human Condensins provides new insights into mitotic chromosome architecture. J. Cell Biol. *217*, 2309–2328.

Wang, B.D., Eyre, D., Basrai, M., Lichten, M., and Strunnikov, A. (2005). Condensin binding at distinct and specific chromosomal sites in the Saccharomyces cerevisiae genome. Mol. Cell. Biol. *25*, 7216–7225.

Wang, X., Brandão, H.B., Le, T.B.K., Laub, M.T., and Rudner, D.Z. (2017). Bacillus subtilis SMC complexes juxtapose chromosome arms as they travel from origin to terminus. Science *355*, 524–527.

Wang, X., Hughes, A.C., Brandão, H.B., Walker, B., Lierz, C., Cochran, J.C., Oakley, M.G., Kruse, A.C., and Rudner, D.Z. (2018). In Vivo Evidence for ATPase-Dependent DNA Translocation by the Bacillus subtilis SMC Condensin Complex. Mol. Cell *71*, 841–847.e5.

Zawadzka, K., Zawadzki, P., Baker, R., Rajasekar, K.V., Wagner, F., Sherratt, D.J., and Arciszewska, L.K. (2018). MukB ATPases are regulated independently by the N- and C-terminal domains of MukF kleisin. eLife *7*, e31522.

STAR★METHODS

KEY RESOURCES TABLE

REAGENT or RESOURCE	SOURCE	IDENTIFIER
Antibodies		
CAP-H	Novus Biologicals	Cat# NBP1-32573
CAP-H2 (Immunofluorescence)	Nishide and Hirano, 2014	N/A
PICH	Abnova	CAT# H9181
CREST	Cortex Biochemistry	CAT# CS1058
MPM2	Millipore	CAT# CV-05-368
SMC4	Bethyl	CAT# A300-064a
CAP-H2 (Western blot)	Bethyl	CAT# A302-275a
Goat anti-Rabbit-PO	DAKO	Cat# P0448
Goat anti-Mouse-PO	DAKO	Cat# P0447
Goat anti-Mouse-488	Molecular probes	Cat# A11029
Goat anti-Rabbit-488	Molecular probes	Cat # A32731
Histone H3 phospho S10	Abcam	Cat# ab5176
Bacterial and Virus Strains		
Competent cells, Alpha-Select Gold Efficiency	GC Biotech	BIO-85027
Chemicals, Peptides, and Recombinant Proteins		
Blasticidin S	Invitrogen	Cat# R210-101
Puromycin	Sigma-Aldrich	Cat# P7255
DAPI	Sigma-Aldrich	Cat# D9542
SiR-DNA	Spicrochrome	CAT# SC007
Vectashield	Vector Laboratories	Cat# H-1000
Sytox Orange	ThermoFisher	Cat# S11368
Streptavidin	ThermoFisher	Cat# 11406452
BSA	ThermoFisher	Cat# 10536735
Biotin-PEG	Laysan Bio	Cat# Biotin-PEG-SVA-5000-1g
PEG	Laysan Bio	Cat# MPEG-SVA-5000-1g
Glucose Oxidase	ThermoFisher	Cat# 11491092
Catalase	Sigma-Aldrich	Cat# C30
Lambda DNA	Promega	Cat# D1521
ATP	ThermoFisher	Cat# R0441
S. cerevisiae/ condensin holocomplex (wild type)	Terakawa et al., 2017	N/A
S. cerevisiae/ condensin holocomplex (Smc2 L1048V)	This paper	N/A
S. cerevisiae/ condensin holocomplex (Smc4 L1323V)	This paper	N/A
S. cerevisiae/ condensin holocomplex (Smc2 Q147L, Smc4 Q302L)	Terakawa et al., 2017	N/A
MPS1 Inhibitor	Reagency	Cat# rgncy-00015
Nocodazole	MP Biomedicals B.V.	Cat# 0215240525
Critical Commercial Assays		
HiSeq SR Cluster Kit v4 cBot	Illumina	Cat# GD-401-4001
Deposited Data		
Hi-C	This paper	GEO: GSE108774
Smc1 head structure	PDB	PDB: 1W1W
Smc3 head structure	PDB	PDB: 4UX3

(*Continued on next page*)

Continued

REAGENT or RESOURCE	SOURCE	IDENTIFIER
Experimental Models: Cell Lines		
HAP1	Carette et al., 2011	N/A
HAP1 *ΔCAP-H2*	This paper	N/A
HAP1 $AS1^{LV}$	This paper	N/A
HAP1 $AS2^{LV}$	This paper	N/A
HAP1 *ΔCAP-H2*/$AS2^{LV}$	This paper	N/A
HAP1 $SMC2^{WT/\Delta}$	This paper	N/A
Oligonucleotides		
SMC2 gRNA Forward: CACCGCTGAACTTAGTGGTGGTCAG	This paper	N/A
SMC2 gRNA Reverse: AAACCTGACCACCACTAAGTTCAGC	This paper	N/A
SMC4 gRNA Forward: CACCGAAGATCTTCAACCTTTCGGG	This paper	N/A
SMC4 gRNA Reverse: AAACCCCGAAAGGTTGAAGATCTTC	This paper	N/A
SMC2 L1085V repair oligo: CAAGGTTGCCTTGGGAAA TACCTGGAAAGAAAACCTAACTGAAGTTAGTGGTGGT CAGAGGTGAGGAATCACTTTGCTATATTATAATTT	This paper	N/A
SMC4 L1191V repair oligo: CAGTGTTCGACCACCTAA GAAAAGTTGGAAAAAGATCTTCAACGTTTCGGGAGG AGAGAAAACACTTAGTTCATTGGCTTTAGTATTTG	This paper	N/A
CAP-H2 targeting CRISPR Forward: CACCGTTCTT GGTGAGGTCGCGGA	This paper	N/A
CAP-H2 targeting CRISPR Reverse: AAACTCCGCG ACCTCACCAAGAAC	This paper	N/A
$SMC2^{WT/\Delta}$ gRNA Forward: CACCGCTTTTATAGGTGGTTATTGG	This paper	N/A
$SMC2^{WT/\Delta}$ gRNA Reverse: AAACCCAATAACCACCTATAAAAGC	This paper	N/A
Recombinant DNA		
6.4-kb plasmid DNA	Cuylen et al., 2011	1288
pX330	Addgene	Cat# 42230
pDonorBlast	Blomen et al., 2015	N/A
pC1-EGFP-CAP-H	Gerlich et al., 2006	N/A
Software and Algorithms		
LAS-AF FRAP-Wizard	Leica	N/A
Fiji	ImageJ	https://imagej.net/Welcome
Prism	GraphPad	https://www.graphpad.com
SoftWorx	Applied Precision	N/A
Crispr design	Zhang Lab	http://zlab.bio/guide-design-resources
HiC-Pro v2.7.7	Servant et al., 2015	N/A
FRAP analysis macro	This paper	N/A
GENOVA V0.9	GitHub	https://github.com/robinweide/GENOVA

LEAD CONTACT AND MATERIALS AVAILABILITY

Further information and requests for resources and reagents should be directed to and will be fulfilled by the Lead Contact, Benjamin D. Rowland (b.rowland@nki.nl).

EXPERIMENTAL MODEL AND SUBJECT DETAILS

Cell line

HAP1 cells (Carette et al., 2011) were cultured at 37°C with 5% CO_2 in IMDM (GIBCO), supplemented with 12% FCS (Clontech), 1% Penicillin/Streptomycin (Invitrogen) and 1% UltraGlutamine (Lonza).

METHOD DETAILS

Genome Editing

To introduce endogenous mutations, CRISPR/Cas9 genome-editing was performed as described (Elbatsh et al., 2016). In brief, guide RNAs (gRNAs) targeting SMC2 and SMC4 were designed using the online CRISPR design tool (http://zlab.bio/guide-design-resources). SMC2 gRNA sequences used: Forward CACCGCTGAACTTAGTGGTGGTCAG, Reverse AAACCTGACC ACCACT AAGTTCAGC. SMC4 gRNA sequences used: Forward CACCGAAGATCTTCAA CCTTTCGGG and Reverse AAACCCCGAAAGGT TGAAGATCTTC. Phosphorylated and annealed oligo's were ligated into pX330 (Addgene plasmid #42230). To introduce the SMC2 L1085V mutation we designed a 90-bp homology-directed donor oligo: for SMC2: CAAGGTTGCCTTGGGAAATACCT GGAAAGAAAACCTAACTGAAGTTAGTGGTGGTCAGAGGTGAGGAATCACTTTGCTATATTATAATTT. For SMC4 L1191V mutation we used a donor oligo: CAGTGTTCGACCACCTAAGAAAAGTTGGAAAAAGATCTTCAACGTTTCGG GAGGAGAGAAAACAC TTAGTTCATTGGCTTTAGTATTTG. To obtain *CAP-H2* knockout cells, Forward CACCGTTCTTGGTGAGGTCGCGGA and Reverse AAACTCCGCGACCTCA CCAAGAAC sgRNAs were cloned into px330. HAP1 clones were generated by insertion of a Blasticidine cassette, as previously described (Haarhuis et al., 2017). 0.1 μg pBabe-Puro was co-transfected (1:10 ratio to CRISPRs) to select for transfected cells using FuGENE 6 (Promega) according to the manufacturer's protocol. Puromycin (2 μg/ml, Sigma-Aldrich) was added to select for transfected cells. Genomic DNA was isolated from picked single clones and the desired mutations were scored for by Sanger sequencing. To obtain the $SMC2^{WT/\Delta}$, diploid HAP1 cells were transfected with sgRNA, Forward: CACCGCTT TTATAGG TGGTTATTGG and Reverse: AAACCCAATAACCACCTATAAAAGC. Heterozygous clones for *SMC2* were identified by Sanger sequencing.

ATPase Assays

The five-subunit wild-type, Smc2 L1048V, Smc4 L1323V, Smc2 Q147L and Smc4 Q302L mutant condensin complexes were expressed and purified from budding yeast, and ATP hydrolysis rates of condensin holocomplexes were measured as described (Terakawa et al., 2017). In short, reactions (10 μl) were prepared with 0.5 μM condensin holocomplex, with or without 24 nM relaxed circular 6.4-kb plasmid DNA in ATPase buffer (40 mM TRIS–HCl pH 7.5, 125 mM NaCl, 10% (v/v) glycerol, 5 mM $MgCl_2$, 5 mM ATP, 1 mM DTT and 33 nM [α^{32}P]-ATP; Hartmann Analytic) and incubated at room temperature (~25°C). One microliter of the reaction mix was spotted onto PEI cellulose F TLC plates (Merck) every 3 min for a total duration of 15 min. Reaction products were resolved using 0.5 M LiCl and 1 M formic acid solution and analyzed on a Typhoon FLA 9,500 scanner (GE Healthcare). ATP hydrolysis rates were calculated from the ADP/ATP ratios from time points in the linear range of the reaction.

Structural Model

The structural model of the ATPase head domains of SMC2-SMC4 heterodimer was generated using the SWISS-MODEL web tool. The model was based on the crystal structures of cohesin's subunits Smc1 (PDB: 1W1W) and Smc3 (PDB: 4UX3).

Immunofluorescence

Cells were grown on 12 mm glass coverslips and pre-extracted using PEM-T buffer (100mM PIPES pH 6.8, 1 mM $MgCl_2$, 5 mM EGTA and 0.2% Triton) for 60 s. Fixation was performed with 4% paraformaldehyde (PFA) for 6 minutes with PEM-T buffer followed by 4 minutes without PFA and blocking was with 3% BSA in PBS for 1 hour. The following antibodies were used: CAP-H (Novus Biologicals), CREST (Cortex Biochem), PICH (Abnova), Histone H3 phospho S10 (Abcam). All antibodies were used at 1:1000 dilution and incubated overnight at 4°C. Secondary antibodies (Molecular probes, Invitrogen) and DAPI were incubated for 1 hour at room temperature. Coverslips were mounted with Vectashield (Vector Laboratories, H-1000). Images were taken using a Deltavision deconvolution microscope (Applied Precision) and image acquisition was done using Softworx (Applied Precision), ImageJ and Photoshop. For the micronuclei assay, HAP1 wild-type cells were treated overnight with 200 nM of an MPS1 inhibitor.

Magnetic Tweezers

Real-time condensin-mediated compaction experiments were done with magnetic tweezers as described (Eeftens et al., 2017). Briefly, a 20kb DNA construct was stretched between a surface and a magnetic bead. All experiments were carried out in 10 mM HEPES-NaOH pH 7.9, 125 mM NaCl, 5mM $MgCl_2$, 1mM DTT. A pre-measurement was taken before addition of protein. Then, condensin wild-type or mutant holocomplexes (10 nM) were added together with ATP (1 mM). Tracking of the beads started immediately after addition of the protein and the force was kept constant throughout all experiments (0.75 pN), except in experiment S3B we increased the force to 1.5 pN. The compaction rate was determined as described (Eeftens et al., 2017).

Single-Molecule Fluorescence Assay

The single-molecule fluorescence assay was performed as described (Ganji et al., 2018). In brief, lambda DNA was immobilized to a PEG-passivated glass surface via streptavidin-biotin linkage at both its ends. The individually distributed tethered DNA was stained with 500 nM Sytox Orange (SxO), (S11368, Thermofisher) for imagining under a home-built wide-field fluorescence microscope using

a 532 nm excitation laser. The process of DNA loop extrusion was monitored upon the addition of condensin (1 or 10 nM according to the experiment) and ATP (5 mM) in condensin buffer (50 mM TRIS-HCl pH 7.5, 50 mM NaCl, 2.5 mM MgCl2, 1 mM DTT) and an oxygen scavenging system. For Figure S4C, the SFM assay was performed with the same salt concentration used in the magnetic tweezer experiment shown in Figure 3 (125 mM NaCl and 5 mM $MgCl_2$). To visualize DNA loops, a constant rate of buffer flow was applied during the course of the experiment with an angle nearly perpendicular to the surface to which DNA is attached.

The rate of DNA loop extrusion was estimated as described previously (Ganji et al., 2018). Briefly, fluorescence intensity kymographs were built from concatenating the normalized intensity profiles of SxO-stained DNA molecules per time point. From the obtained kymographs, the position of the loop at each time point was found by center-of-mass tracking along the length of DNA molecule. Subsequently, the DNA loop size was calculated by integrating the intensity from 11 pixels cantered at the position of the loop and multiplying it by the length of lambda DNA (48.502 kbp) per time point. Finally, the rate for DNA loop extrusion was determined from the slope of linear DNA size increase observed in the first 10 s of the DNA loop extrusion.

The observed separate loops and higher-order structures as shown in Figures 4B–4D were well-distinguishable to each other in our experiments. The separate loops were observed as two local maxima along the otherwise homogeneous fluorescence intensity of the DNA molecule, while the higher-order DNA structures appeared as an elongated line of high fluorescence intensity that stretched along the length of DNA. The 'disruption' event of separate loops or higher-order structures shown in Figure 4C was defined as an event from which their respective characteristic structures are disappeared, namely, a release of one or both of the DNA loops into an initial bare DNA and a release of the elongated structure into a single loop, for separate loops and higher-order structure, respectively. Statistical analysis was performed using GraphPad Prism 8 software. The applied statistical method and *P values* are reported in the figure legends. Statistical significance is categorized as follows: $^{**}p < 0.01$ and $^{****}p < 0.0001$.

Hi-C

Cells were plated in T175 flasks (Cellstar, Greiner bio-one). The next day, cells were treated with nocodazole for 1.5 hours and mitotic cells were collected by shake-off. Cells were cross-linked with 2% formaldehyde, blocked with 3% BSA in PBS with Tween 0.1% (PBST) and then incubated with the mitosis-specific antibody MPM2 (1:500, Millipore) overnight at 4°C. Cells were washed with PBST then incubated with the secondary Alexafluor antibody. Labeled mitotic cells were sorted by FACS (BD FASAira II, BD biosciences). 5-10 million sorted cells were treated with 0.1% SDS final concentration (5μl 10% SDS per 500μl volume) and incubated for 10 minutes at 65°C. Then 30μl 20% Triton X-100 (Sigma-Aldrich) was added to the cells (final concentration = 1% Triton X-100). The subsequent sample preparation steps were done as described (Haarhuis et al., 2017). Raw sequence data was mapped and processed using HiC-Pro v2.9 (Servant et al., 2015). Data was mapped to hg19. The relative contact probability was computed as previously described (Haarhuis et al., 2017).

Chromosome Spreads

Cells were treated with nocodazole for 1.5 hours and mitotic cells were collected by shake-off. Cells were incubated with 75 mM KCl for 20 minutes. Cell pellets were twice resuspended in fixative solution (Methanol: Acetic Acid, 3:1) and spun down. Fixed cells were incubated with DAPI and dropped on tilted cover slides, and then dried at 37°C. Dried slides were mounted with Vectashield (Vector Laboratories, H-1000). Images of spreads were taken using the Metafer system (Metasystems).

Live-Cell Imaging

Cells were grown on 8-well glass-bottom dishes (LabTek). Two hours prior to imaging, SiR-DNA probe (1:2000, Spirochrome) was added together with verapamil (1:10000) to visualize DNA in L-15 CO_2-independent medium (GIBCO). Images were taken using a Deltavision deconvolution microscope (Applied Precision). Cells were imaged every 5 minutes using a 40x air objective with 3 × 3 μm Z stacks. Image acquisition was carried out using Softworx (Applied Precision) and ImageJ.

Fluorescence Recovery After Photobleaching (FRAP) Assays

Cells were transfected with a pC1-EGFP-CAP-H construct in 4-well glass bottom dishes (LabTek). 48 hours post-transfection, SiR-DNA probe (1:2000, Spirochrome) was added to cells to visualize DNA, in L-15 CO_2-independent medium (GIBCO). FRAP experiments were performed using a confocal microscope (Leica Microsystems) with a 63x oil immersion objective using the LAS-AF FRAP-Wizard. Images were taken by accumulating 4 frames at a scanning speed of 1000 Hz. Photobleaching was performed by 6 times illuminating the selected region at 100-fold laser power (488 nm Laser). 60 post-bleaching images were taken with 10 s intervals. Analysis of images was done using an in-house ImageJ macro. A mask on the DNA signal was created and the EGFP-CAP-H signal was normalized to the DNA signal.

Western Blotting

Cells were grown in 6-well plates, harvested and lysed with Laemmli buffer (120 mM Tris pH 6.8, 4% SDS, 20% glycerol) by boiling at 95°C for 5 minutes. Total protein concentration was determined with Lowry assays and protein levels were analyzed with western blotting. The following antibodies were used: SMC4 (1:5000 Bethyl) and CAP-H2 (1:1000, Bethyl).

QUANTIFICATION AND STATISTICAL ANALYSIS

Statistical details of experiments can be found in the figure legends or Method Details section.

DATA AND CODE AVAILABILITY

Software used for Hi-C data analysis can be found at: https://github.com/robinweide/GENOVA.

The accession number for the data for Hi-C reported in this paper is NCBI GEO: GSE108774.